Confining Standing Waves in Optical Corrals

Yelizaveta Babayan,[†] Jeffrey M. McMahon,[†,§] Shuzhou Li,[†] Stephen K. Gray,[§] George C. Schatz,[†] and Teri W. Odom[†,‡,*]

[†]Department of Chemistry and [‡]Department of Materials Science and Engineering, Northwestern University, 2145 Sheridan Road, Evanston, Illinois 60208-3113, and [§]Chemical Sciences and Engineering Division, Argonne National Laboratory, Argonne, Illinois 60439

ABSTRACT Near-field scanning optical microscopy images of solid wall, circular, and elliptical microscale corrals show standing wave patterns confined inside the structures with a wavelength close to that of the incident light. The patterns inside the corrals can be tuned by changing the size and material of the walls, the wavelength of incident light, and polarization direction for elliptical corrals. Finite-difference time-domain calculations of the corral structures agree with the experimental observations and reveal that the electric and magnetic field intensities are out of phase inside the corral. A theoretical modal analysis indicates that the fields inside the corrals can be attributed to p- and s-polarized waveguide modes, and that the superposition of the propagating and evanescent modes can explain the phase differences between the fields. These experimental and theoretical results demonstrate that electromagnetic fields on a dielectric surface can be controlled in a predictable manner.

KEYWORDS: near-field scanning optical microscopy · metal microstructures · finite-difference time-domain calculations · dephasing · waveguide modes

Metallic structures that can confine and manipulate light on surfaces are of interest for discovering novel ways to control light and for emerging applications in optoelectronics,[1] photonics,[1−3] and chemical and biological sensing.[4,5] One type of structure that has been used to confine light on a dielectric surface is an optical corral,[6] a microscale (1−10 μm) analogue of the nanoscale quantum corral.[7] Calculations performed on an optical corral made from dielectric pads arranged in a ~3 μm diameter circle have shown that confined electromagnetic waves can generate patterns that resemble those of their electronic counterparts.[6] Near-field scanning optical microscopy (NSOM) has also been used to observe confined photonic states within structures composed of 100 nm diameter Au posts (also 100 nm high) arranged in a 3.6 μm diameter circle on an indium tin oxide (ITO) substrate.[8] Confined electromagnetic waves in a 4 μm × 2 μm structure composed of 100 nm Au posts were also measured.[8] These optical corrals make possible new fundamental studies of light propagation in confined geometries on dielectric surfaces.

In this article, we describe the near-field optical characterization and modeling of lithographically patterned arrays of micron-sized metallic circular rings and ellipses. Because these structures have solid walls, they can confine light within their interior more effectively than walls composed of particles. Only certain wavelengths of light, however, were found to be efficiently sustained inside the circular corrals to produce a bright spot at their center. Elliptical corrals with three different eccentricities ($e = (1 - b^2/a^2)^{1/2}$, where a and b are the long and short axes, respectively) were also investigated for their ability to tailor the standing wave patterns by varying the polarization of the incident light. Unlike in the quantum corral,[7,9,10] polarization effects can be used to control the patterns of the standing waves inside elliptical corrals. NSOM measurements also revealed that ellipses with larger eccentricities have the ability to modulate light at the focal points to produce bright or dark spots depending on the wavelength of the incident light.

Finite-difference time-domain (FDTD) calculations of the intensities of the electric field ($\vec{E}^2$) and magnetic field ($\vec{H}^2$) inside the corrals supported the experimental results, and the standing wave patterns were seen to depend on the inclusion of the ITO substrate. In addition, we found that the electric and magnetic field intensities were out of phase within the corrals. Using insight gained from our previous study on the dephasing of electric and magnetic fields inside micron diameter slits,[11] we can explain the corral results as a superposition of propagating and evanescent p- and s-polarized waveguide modes. Importantly, this modal analysis enables a straightforward understanding of the relation

See the accompanying Perspective by Nordlander on p 488.

*Address correspondence to todom@northwestern.edu.

Received for review December 15, 2008 and accepted February 13, 2009.

Published online February 25, 2009.
10.1021/nn8008596 CCC: $40.75

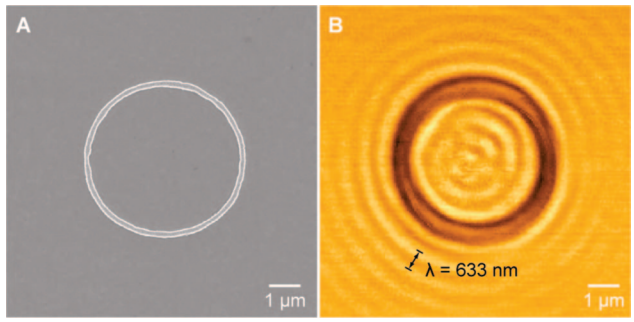

Figure 1. Circular optical corrals. (A) SEM image of a 4.8 μm diameter Au corral. (B) NSOM image of (A) under circularly polarized 633 nm incident light.

between the NSOM measurements and the electric and magnetic fields that are typically used to interpret such near-field images.

RESULTS AND DISCUSSION

Circular Corrals. Figure 1A shows a single circular corral made of Au with an inside diameter of 4.8 μm imaged by collection mode NSOM. When the structure was illuminated at normal incidence with circularly polarized 633 nm light, two specific features were found inside and around the corral: (1) evanescent waves with ~200−250 nm amplitude in the *z*-direction (normal to the surface of the sample), which were quantified by single-point NSOM spectroscopy, and (2) standing wave patterns inside and outside of the structure with a wavelength close to that of the light used for imaging (Figure 1B). The pattern inside the corral contained ripples, while the pattern outside consisted of concentric, circular fringes.

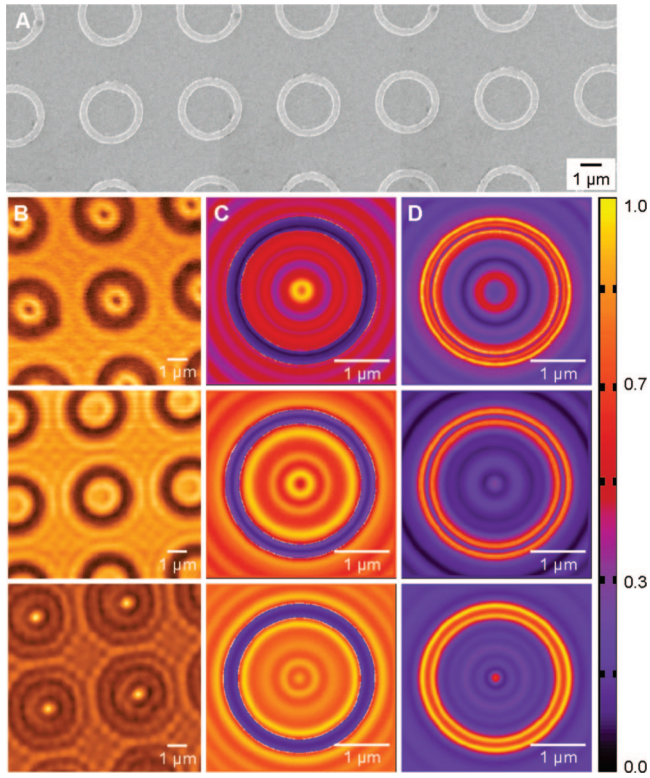

Figure 2. Wavelength dependence of standing wave patterns in circular corrals. (A) SEM image of arrays of 2.23 μm diameter Au corrals. (B) Collection mode NSOM images under (top) 633 nm light, (middle) 543 nm light, and (bottom) 457 nm light. FDTD calculations of (C) $\vec{E}^2$ and (D) $\vec{H}^2$ under the same conditions as (B).

To investigate the effect of corral size on the patterns, we fabricated arrays of Au circular corrals with inner diameters of 2.23 and 5 μm center-to-center separations (Figure 2A). When these structures were imaged using circularly polarized 633 nm light, the number of internal ripples decreased (Figure 2B, top) as expected, and the central spots inside the corrals became dark. These results are similar to those observed in NSOM images of the local density of states inside 2.7 μm circular, Au discrete wall corrals.[12] In addition, the standing wave pattern outside of the corrals became more well-defined. FDTD calculations of $\vec{E}^2$ and $\vec{H}^2$ (Figures 2C,D, top) were carried out for the 2.23 μm circular Au corral using 633 nm incident light. Good agreement between experimental and calculated $\vec{E}^2$ patterns was observed both inside and around the corral, including the peak-to-peak wavelength of the standing waves and positions of the maxima and minima. Changes in the intensity and pattern of the standing waves outside of the corrals are easily explained as diffraction between opposite corral walls from both individual and neighboring corrals, where the longer wavelengths correspond to lower diffraction orders and are thus more intense. However, the fields inside the corrals were found to only depend on the geometry and local dielectric environment of an individual corral. For example, calculations without the ITO substrate produced significantly different field patterns inside and around the corral (Figure S1 in the Supporting Information). The primary reason for this difference is that the effective incident wavelength on the corrals depends on the substrate, $\lambda_{eff} = \lambda_0\sqrt{\varepsilon_{sub}}$, where λ_{eff} is the effective incident wavelength and λ_0 is the actual incident wavelength inside the substrate with permittivity ε_{sub}. Presumably, the field patterns will be completely reversed when $d/\lambda_0 - d/\lambda_0\sqrt{\varepsilon_{sub}} = n + 1/2$, where d is the corral diameter and $n = 0, 1, 2,...$ Interestingly, $\vec{E}^2$ and $\vec{H}^2$ were found to be out of phase within the corral, which can be explained using a waveguide modal analysis.[11,13] For simplicity, we replaced the circular corral by a 1D slit structure with a width d that is the same diameter as the corral; thus, the electromagnetic field was completely defined by specifying only the transverse component. Assuming that Au can be treated as a perfect electric conductor (PEC), a material in which the dielectric constant is infinite, the transverse component of the field inside the corral can be expanded as a superposition of the eigenmodes of a 1D waveguide. For p-polarization, where the transverse axis is the *z*-axis, this expansion becomes

$$H_z = \sum_{m=0}^{\infty} (A_m e^{i\beta_m y} + B_m e^{-i\beta_m y})\phi_m(x) \qquad (1)$$

where $\beta_m = \sqrt{k_0^2\varepsilon_s - (m\pi/d)^2}$ is the waveguide wavevector magnitude, $k_0 = 2\pi/\lambda_0$ is the incident wavevector magnitude, ε_s is the permittivity inside the slit, A_m and B_m are amplitudes of the m^{th} mode, and $\phi_m(x) = (2/\sqrt{d})\cos(m\pi(x + d/2)/d)$ is the solution to the Helmholtz equation within the slit subject to PEC boundary conditions at $x = \pm d/2$. By applying boundary conditions across the interfaces and projecting the resulting equations onto a set of plane waves, the amplitudes of each mode can be determined. We have previously found that for a 2.23 μm slit in a 60 nm thick film illuminated with p-polarized 543 nm light the coefficients are mainly composed of the propagating $m = 0$ mode and the evanescent $m = 8$ mode (*i.e.*, a mode in which β_m is entirely imaginary), which means that scattering by the slit (corral) induces a modal transition from propagating to evanescent.[11] The transitional evanescent mode corresponds to light that propagates parallel to the surface with a wavelength just slightly longer than the incident light ($m\pi/d \approx k_0\sqrt{\varepsilon_s}$), which explains the similarity between this wavelength and the peak-to-peak separation of the standing waves, as well as their evanescent character seen in the experiments. Furthermore, the superposition of higher order evanescent modes onto the propagating modes explains the out of phase behavior of $\vec{E}^2$ and $\vec{H}^2$. To fully describe the experimental results, however, s-polarization, which has a similar solution to eq 1 with H_z replaced by E_z, also needs to be taken into account.

Variations of the standing wave patterns in response to a change in the wavelength of the light were also observed. The 2.23 μm corrals were illuminated and imaged using two additional wavelengths, 543 and 457 nm (Figure 2B,C, middle and bottom). When the 633 nm light was replaced with 543 nm, and then with 457 nm, the dark spot in the middle of the corral gradually switched to a bright spot (Figure 2B, bottom), which had an intensity ~6 times higher than the lowest intensity spot. This observation suggested that only certain wavelengths of light were optimally sustained inside the corrals to produce a high intensity spot at their center. Interestingly, the patterns formed within the optical corrals resembled the patterns of electronic standing waves in quantum corrals.[7,9,10]

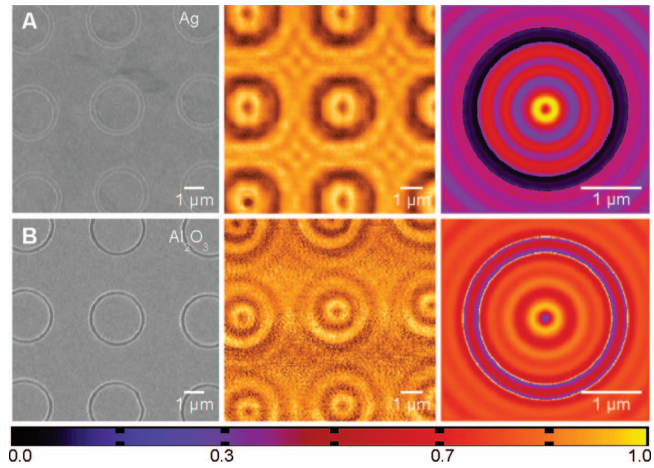

Figure 3. Materials dependence of standing wave patterns. SEM, NSOM, and FDTD-calculated $\vec{E}^2$ images for (A) Ag and (B) Al_2O_3 corrals illuminated using 633 nm light.

To investigate the effect of the corral material on the patterns, we fabricated circular corrals with Ag and dielectric (Al_2O_3) walls with inside diameters of 2.35 μm (Figure 3). When the corrals were excited with circularly polarized 633 nm light, identical patterns were produced inside of the metallic (Figure 3A) and the dielec-

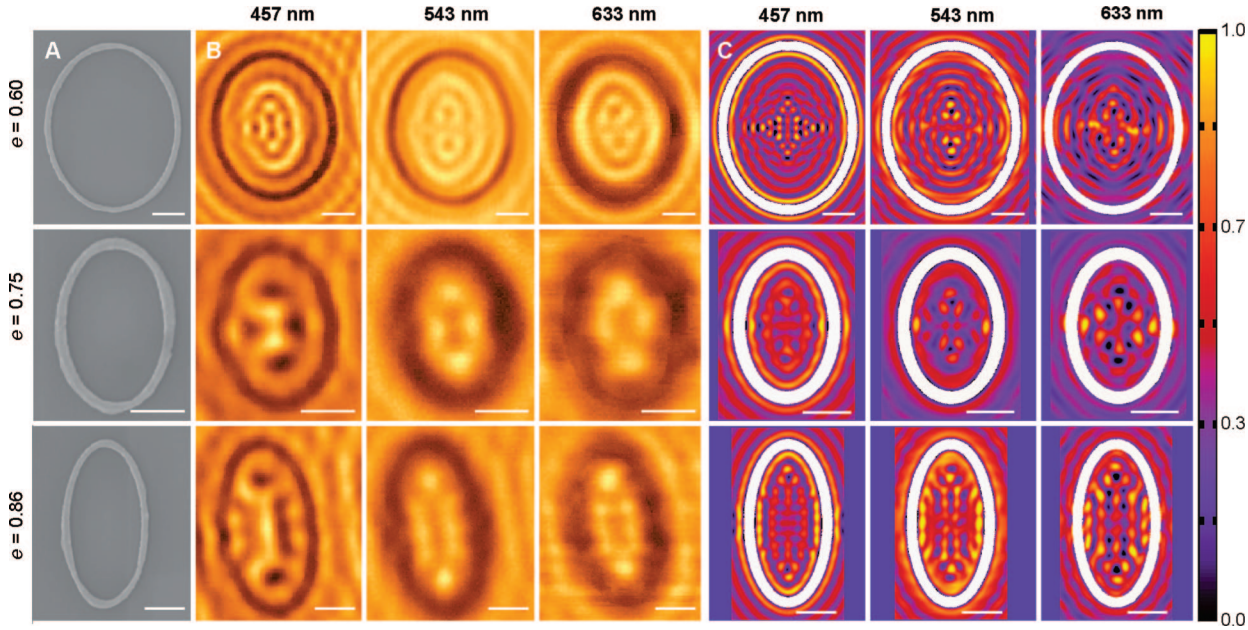

Figure 4. Effect of the ellipse shape on the patterned waves. (A) SEM images of ellipses with eccentricities of (top) 0.60, (middle) 0.75, and (bottom) 0.86. (B) NSOM images acquired using circularly polarized light for (A). (C) FDTD calculations of $\vec{E}^2$ for (A). All scale bars are 1 μm.

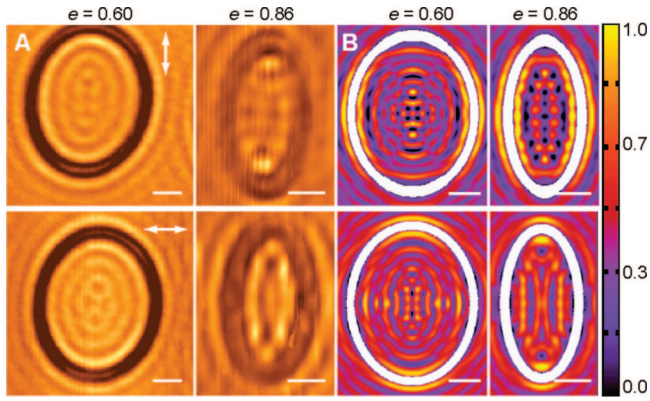

Figure 5. Polarization effects on standing wave patterns. (A) Ellipses with $e = 0.60$ and 0.86 imaged using 543 nm light with linear polarization, along the long axis (top) or short axis (bottom). (B) FDTD calculations of $\vec{E}^2$, with the ellipses outlined in white. All scale bars are 1 μm.

tric structures (Figure 3B). The dielectric rings, however, were brighter than the metallic ones, which was expected because Al_2O_3 is transparent. Another variation between the optical images was in the contrast of the pattern of the standing waves, which indicated that the reflectivity of the corral material was important. The analysis based on $\phi_m(x)$ (and the equivalent expression for s-polarization) is also better satisfied as the reflectivity (or equivalently, the dielectric constant) goes to infinity. As expected, the dielectric structures had the lowest contrast because the reflectivity of Al_2O_3 compared to the metals is lower at 633 nm. Between the two metals, Ag had a slightly better contrast because it has ~5% higher reflectivity at 633 nm than Au.[14] FDTD calculations of $\vec{E}^2$ for these corrals supported the experimentally observed results (Figure 3).

Elliptical Corrals. Although circular corrals provide a simple platform for studying the optical analogue to the quantum corral, more complex structures provide additional ways to manipulate light on dielectric surfaces. For example, structures with lower symmetries provide unique opportunities to study polarization effects on light confinement within the corral structures. Figure 4A shows ellipses with eccentricities of $e = 0.60$ ($a = 2.5$ μm, $b = 2$ μm), $e = 0.86$ ($a = 2$ μm, $b = 1$ μm), and $e = 0.75$ ($a = 1.5$ μm, $b = 1$ μm). Upon illumination of the $e = 0.60$ ellipses with circularly polarized 457 nm light, complex patterns, which resembled those of the quantum corrals of similar eccentricity,[9] were formed inside the structures (Figure 4B). Interestingly, ellipses with $e = 0.75$ and 0.86 suppressed light at the focal points (dark spots were present), while the ellipse with $e = 0.60$ did not. To investigate whether this phenomenon was related to the structure of the corral or to the wavelength of light used for imaging, the ellipses were also imaged with 543 and 633 nm light (Figure 4B). For these wavelengths, the ellipses with larger eccentricities showed bright spots at the focal points. These effects can be explained in manner analogous to the circular corrals, where waveguide modes are excited by the short and long axes of the corrals to create an interference pattern. These results demonstrate that the standing wave patterns can be controlled by changing the shape of the corral as well as the excitation wavelength of light.

FDTD calculations were carried out for the elliptical corrals excited with circularly polarized light (Figure 4C). As with the circular corrals, $\vec{E}^2$ agreed well with experiment, and $\vec{E}^2$ and $\vec{H}^2$ were seen to be out of phase (not shown). Because of the low symmetry of the elliptical corrals, we expected the fields confined within the structures to exhibit polarization dependence. The $e = 0.60$ and 0.86 ellipses were imaged using linearly polarized (along either the short or long axis) 543 nm light (Figure 5A). FDTD calculations were also carried out for the elliptical corrals excited with linearly polarized light (Figure 5B) and supported the experimentally observed trends. These results confirmed that the standing wave patterns can be tailored by simply changing the polarization direction of the incident light and can be explained using the same analysis applied to the circular corrals. In the elliptical corrals, however, for linearly polarized light, an asymmetric excitation of p- and s-polarized waveguide modes occurs, and the FDTD results show that the s-polarized waveguide mode is dominant.

CONCLUSIONS

We have presented a method for confining electromagnetic waves in artificial microscale structures and demonstrated that optical analogues of the quantum corral can be created. Using circular corrals, we showed that only certain wavelengths of light exhibited constructive interference to produce a bright spot at their centers. The ability to modify the standing wave patterns of light inside the corrals was further investigated in elliptical structures, which allowed the patterns to be tailored by simply changing the polarization of the incident light. Wavelength-dependent changes of the patterns were also observed. Ellipses with different eccentricities were investigated to understand the size and shape dependence of the corral structure on the patterns. Interestingly, ellipses with larger eccentricities showed that light can either be suppressed or enhanced at the focal points depending on the excitation wavelength.

The NSOM measurements were in good agreement with FDTD calculations, which revealed that the electric field intensities matched the measurements and that the magnetic field intensities were $\pi/2$ out of phase. The origin of the standing wave patterns, and dephasing, could be explained using a simple waveguide model. In particular, light scattering from the corrals produces evanescent waveguide modes at the dielectric interface with an effective wavelength similar to that of the incident light, which when

superimposed onto propagating waveguide modes leads to a dephasing of the electric and magnetic field intensities. These results are important for interpreting NSOM measurements since the power flow (the property that is directly probed) depends on both the electric and magnetic fields.

METHODS

Fabrication of Optical Corrals. Optical corrals (circular and elliptical) on ITO-coated glass (thin film devices) were fabricated using lithographic techniques. Polymeric templates with arrays of circular rings with ~250 nm widths and inner diameters of ~2.23 and ~4.8 μm were fabricated using phase-shifting photolithography (PSP). The center-to-center spacing was 4.5 μm for the smaller corrals and 15 μm for the larger corrals. Electron-beam lithography (EBL) was used to fabricate the templates for the elliptical corrals with ~250 nm widths and 0.60, 0.75, and 0.86 eccentricities. These eccentricities were chosen to mimic the sizes of the quantum mirage structures.[10] EBL was used instead of PSP for the elliptical corrals because it allowed for fabrication of structures with different sizes on the same substrate.

The corrals were produced by depositing 50−60 nm of Au into the resist templates fabricated by PSP and EBL and then performing lift-off. The height of the structures was chosen to be larger than the skin depth of Au at optical wavelengths (~25 nm).[15] Metal deposition was accomplished using an e-beam evaporator (PVD 75, Kurt J. Lesker) with a base pressure of 10^{-7}−10^{-6} Torr. The thickness of the film and the deposition rate, which was maintained at ~1 Å/s to create a smooth film, were monitored using a 6 MHz gold microbalance (Kurt J. Lesker). The substrates were sonicated in acetone or Shipley remover 1165 to remove the resist and leave the Au structures on the ITO substrate. Circular corrals made from Ag and alumina (Al_2O_3) were also fabricated in a similar manner. For Au and Ag structures, 5 nm of Cr was deposited as an adhesion layer.

Near-Field Scanning Optical Microscopy. NSOM measurements were performed using an Aurora 3 (Veeco) instrument using commercial Al-coated, pulled, fiber optic probes with 100−150 nm apertures and 80−100 kHz resonant frequencies. The samples were uniformly illuminated through a 40X objective lens (Olympus), and the light from the sample was collected through the probe into a high quantum efficiency avalanche photodiode (SPCM-AQR-14, Perkin-Elmer). A focusing lens was positioned before the objective lens to decrease the divergence of the light as well as create a <0.5 mm uniform illumination spot on the surface of the sample. Three different sources were used for illumination: 457 nm Ar ion (2−10 mW, LaserPhysics), 543 nm HeNe (5 mW, Melles Griot), and 633 nm HeNe (15 mW, Melles Griot) lasers. Both linearly and circularly polarized light was used to study the corrals. Linearly polarized laser light was converted into circularly polarized light by placing a 1/4-waveplate in front of the laser source; a 1/2-waveplate was used to change the angle of polarization with respect to the sample.

Theoretical Methods. FDTD calculations were performed using standard techniques.[16] Isolated corrals were modeled after the experiments as 60 nm high and 250 nm wide Au, Ag, or Al_2O_3 corrals on top of a 150 nm thick $n = 2.0$ layer (similar to ITO), all on top of a glass ($n = 1.5$) substrate. (2D FDTD calculations of analogous systems indicated that isolated corrals produced results similar to those of a periodic array of corrals.) The computational domain was discretized using grid spacings of 5.0 nm and terminated with convolutional perfectly matched layers (CPML). The dielectric functions of Au and Ag were modeled using Drude plus 2 Lorentz pole functions, accurately fit to empirically determined dielectric data for wavelengths relevant in this work (400−700 nm). The parameters for Au have been reported previously,[17] and those for Ag are given in the Supporting Information. Al_2O_3 was assumed to have a constant refractive index of $n = 1.77$. A Gaussian damped sinusoidal pulse, chosen to have wavelength content over the range of interest, was introduced into the computational domain using the total field-scattered field technique at normal incidence from the glass substrate. Field measurements were made 20 nm above the $n = 2.0$ layer by Fourier transforming the time-domain electric and magnetic fields.

FDTD calculations without the substrate, which plays an important role in determining the maxima and minima positions of the electric and magnetic field intensities, are presented in the Supporting Information. In addition, discrete dipole approximation (DDA)[18] calculations for many of the structures studied using FDTD (but without the substrate) are also presented.

Acknowledgment. This work was supported by the NSF MRSEC program at Northwestern University (DMR-0520513), the David and Lucile Packard Foundation, the U.S. Department of Energy (DEFG02-03-ER15487), and the NSF (DMR-0705741). S.K.G. was supported by the U.S. Department of Energy, Office of Basic Energy Sciences, Division of Chemical Sciences, Geosciences, and Biosciences under contract DE-AC02-06CH11357. This research used resources of the National Energy Research Scientific Computing Center, which is supported by the Office of Science of the U.S. Department of Energy Contract DE-AC02-05CH11231.

Supporting Information Available: Drude plus 2 Lorentz pole dielectric mode used in the FDTD calculations, with parameters for Ag; FDTD calculations without the ITO substrate; DDA calculations of the corrals. This material is available free of charge *via* the Internet at http://pubs.acs.org.

REFERENCES AND NOTES

1. Barnes, W. L.; Dereux, A.; Ebbesen, T. W. Surface Plasmon Subwavelength Optics. *Nature* **2003**, *424*, 824–830.
2. Ebbesen, T. W.; Lezec, H. J.; Ghaemi, H. F.; Thio, T.; Wolff, P. A. Extraordinary Optical Transmission through Subwavelength Hole Arrays. *Nature* **1998**, *391*, 667–669.
3. Ozbay, E. Plasmonics: Merging Photonics and Electronics at Nanoscale Dimensions. *Science* **2006**, *311*, 189–193.
4. Haes, A. J.; Haynes, C. L.; McFarland, A. D.; Schatz, G. C.; Van Duyne, R. P.; Zou, S. Plasmonic Materials for Surface-Enhanced Sensing and Spectroscopy. *MRS Bull.* **2005**, *30*, 368–375.
5. Willets, K. A.; Van Duyne, R. P. Localized Surface Plasmon Resonance Spectroscopy and Sensing. *Annu. Rev. Phys. Chem.* **2007**, *58*, 267–297.
6. Colas des Francs, G.; Girard, C.; Weeber, J.-C.; Chicane, C.; David, T.; Dereux, A.; Peyrade, D. Optical Analogy to Electronic Quantum Corrals. *Phys. Rev. Lett.* **2001**, *86*, 4950–4953.
7. Crommie, M. F.; Lutz, C. P.; Eigler, D. M. Confinement of Electrons to Quantum Corrals on a Metal Surface. *Science* **1993**, *262*, 218–220.
8. Chicanne, C.; David, T.; Quidant, R.; Weeber, J. C.; Lacroute, Y.; Bourillot, E.; Dereux, A.; Colas des Francs, G.; Girard, C. Imaging the Local Density of States of Optical Corrals. *Phys. Rev. Lett.* **2002**, *88*, 097402/1–097402/4.
9. Fiete, G. A.; Heller, E. J. Colloquium: Theory of Quantum Corrals and Quantum Mirages. *Rev. Mod. Phys.* **2003**, *75*, 933–948.
10. Manoharan, H. C.; Lutz, C. P.; Eigler, D. M. Quantum Mirages Formed by Coherent Projection of Electronic Structure. *Nature* **2000**, *403*, 512–515.
11. McMahon, J. M.; Gray, S. K.; Schatz, G. C. Dephasing of Electromagnetic Fields in Scattering from an Isolated Slit in a Gold Film. In *Plasmonics: Nanoimaging, Nanofabrication, and Their Applications IV*; Proceedings of SPIE, 2008, San Diego, CA; Vol. 7033, pp 703311/1−703311/6.

12. Dereux, A.; Girard, C.; Chicanne, C.; des Francs, G. C.; David, T.; Bourillot, E.; Lacroute, Y.; Weeber, J. C. Subwavelength Mapping of Surface Photonic States. *Nanotechnology* **2003**, *14*, 935–938.
13. Bravo-Abad, J.; Martin-Moreno, L.; Garcia-Vidal, F. J. Transmission Properties of a Single Metallic Slit: From the Subwavelength Regime to the Geometrical-Optics Limits. *Phys. Rev. E* **2004**, *69*, 026601-1–026601-6.
14. Johnson, P. B.; Christy, R. W. Optical Constants of the Noble Metals. *Phys. Rev. B* **1972**, *6*, 4370–4379.
15. Dawson, P.; Boyle, M. G. Light Emission from Scanning Tunneling Microscope on Polycrystalline Au Films: What is Happening at the Single-Grain Level? *J. Opt. A:* **2006**, *8*, S219–S226.
16. Taflove, A.; Hagness, S. C. *Computational Electrodynamics: The Finite-Difference Time-Domain Method*, 3rd ed.; Artech House, Inc.: Norwood, MA, 2005.
17. McMahon, J.; Henzie, J.; Odom, T. W.; Schatz, G. C.; Gray, S. K. Tailoring the Sensing Capabilities of Nanohole Arrays in Gold Films with Rayleigh Anomaly-Surface Plasmon Polaritons. *Opt. Exp.* **2007**, *15*, 18119–18129.
18. Draine, B. T.; Flatau, P. J. Discrete-Dipole Approximation for Scattering Calculations. *J. Opt. Soc. Am. A* **1994**, *11*, 1491–1499.